The Journal of International Advanced Otology

J Int Adv Otol 2019; 15(1): 77-82 • DOI: 10.5152/iao.2019.6246

Original Article

Human Inner-ear Malformation Types Captured in 3D

Anandhan Dhanasingh, Aarno Dietz, Claude Jolly, Peter Roland

MED-EL GmbH, Implants, Innsbruck, Austria (AD, CJ)
Department of Otolaryngology, Kuopio University Hospital, Kuopio, Finland (AD)
Department of Otolaryngology, Universtiy of Texas Southwestern Medical Center, Dallas, USA (PR)

ORCID IDs of the authors: A.D. 0000-0003-2116-9318; A.D. 0000-0001-6076-1037; C.J. 0000-0002-4886-3759; P.R. 0000-0002-4272-3026.

Cite this article as: Dhanasingh A, Dietz A, Jolly C, Roland P. Human Inner-ear Malformation Types Captured in 3D. J Int Adv Otol 2019; 15(1): 77-82.

OBJECTIVES: Capture the human inner-ear malformation types in 3D by segmenting the inner-ear structures from clinical CT (computed tomography) and MR (magnetic resonance) image datasets. Volumetric analysis was done to find the variations in the volume of cochlear part alone from complete inner-ear followed by 3D printing from the 3D segmented models.

MATERIALS AND METHODS: Using 3D slicer freeware, the complete inner-ear structures were segmented from anonymized CT and MR image by setting a tight grey-scale threshold to avoid capturing unwanted structures followed by volumetric analysis of the cochlear part alone. 3D printing was done using Form labs desktop 3D printer.

RESULTS: We identified 2x normal anatomy (NA) cochlea, 1x enlarged vestibular aqueduct syndrome (EVAS), 3x incomplete partition (IP) type-I, 4x IP type-II, 3x IP type-III, 5x common cavity (CC) and 5x cochlear hypoplasia (CH). 3D segmented models along with the 3D printed models showed huge variation in size, shape and the anatomy among the image data-sets analyzed. Volumetric analysis showed that on average, volume of CC was above 150mm3, volume of CH fell below 80mm3, Volume of NA, EVAS and IP-I were all around 85-105mm3 whereas the volume of IP-II was around 50mm3.

CONCLUSION: Visualizing human inner-ear malformation types in 3D both as computer models and as 3D printed models is a whole-new experience as demonstrated in this study. The volumetric analysis showed a huge variation among the volume of cochlear part alone among the malformation types.

KEYWORDS: Three dimensional visualization, enlarged vestibular aqueduct syndrome, incomplete partition, common cavity, cochlear hypoplasia

INTRODUCTION

Cochlear implantation (CI) is a widely accepted and the only solution to date for treatment of severe to profound sensorineural hearing loss [1]. Variation in cochlear morphology is not just in size, shape, and the coiling geometry but also in the internal anatomy of cochlea [2]. As per literature, approximately 20% of cochlear implant population has some degree of malformation in cochlear anatomy [3, 4]. A new classification of inner-ear malformations, proposed by Sennaroglu et al. [5], has been widely accepted. Accurate identification of the type of malformation is necessary for adequate surgical planning. It is obtained by careful analysis of the pre-operative imaging. The CI surgery in cases of inner-ear malformation is challenging because the grossly altered anatomy including clear surgical landmarks such as lateral semi-circular canal (SCC), facial nerve, and cochlear promontory are often absent. Literature reporting on the placement of electrode in SCC and internal auditory canal (IAC) [6] that were identified with intra-operative radiographs and corrected in the same surgery conveys us the message that more pre-operative planning methods are necessary.

Depending on the types of malformation, hearing outcomes with CI in cases of inner-ear malformation vary [7-12]; higher the degree of malformation, poorer the expected hearing performance with the CI. Three-dimensional (3D) models of the malformed anatomical structures can help in several aspects including from an educational perspective, surgical planning, from research perspective [13] and to have a better clinician-patient communication especially to understand the pathology and procedure [14]. Considering the high cost of CI that is covered either privately by the patient or by the health insurance companies and the physical pain from the surgery tolerated by the patient, it makes absolute sense to have additional effort in pre-operative planning.

This study was presented at the 15th International conference on cochlear implants and other implantable auditory technology, 27-30 June 2018, Antwerp, Belgium and 55th Inner Ear Biology Workshop, 6-8 September 2018, Berlin, Germany.

Corresponding Address: Anandhan Dhanasingh E-mail: anandhan.dhanasingh@medel.com

Submitted: 24.10.2018 • **Revision Received:** 02.01.2019 • **Accepted:** 03.03.2019

©Copyright 2019 by The European Academy of Otology and Neurotology and The Politzer Society - Available online at www.advancedotology.org

This article captures human inner-ear malformation types in 3D by segmenting the inner-ear from the clinical high-resolution computed tomography (HRCT) and/or magnetic resonance imaging (MRI) data sets. The secondary aim is to have a better understanding and visualization of size, shape, and the availability of cochlea, vestibule, vestibular aqueduct (VA), SCCs, and IAC by 3D printing it from 3D segmented models.

MATERIALS AND METHODS

Anonymized pre-operative HRCT and MR image data sets of human temporal bones with a variety of inner-ear malformations were provided for educational purposes by several clinics across the world from the year 2011 to 2018. An MRI data set was used only for third sample under cochlear hypoplasia given in Table 2, for which CT data set was not available. The image data sets were loaded into 3D slicer freeware (3D Slicer, https://www.slicer.org/; version 4.8.0, Massachusetts, USA) followed by segmentation of cochlea along with IAC, vestibular organ, and VA. Segmentation of these structures was performed as precisely as possible in axial plane in every slice the inner-ear structures were seen by setting tight thresholds of the grayscale to avoid capturing undesired structures (refer Figure 1). Grayscale thresholding to capture the desired structures was done individually for every individual image data set by the first author and was verified by both the second and fourth authors, both otolaryngologists by profession. Figure 1 shows an example of grayscale thresholding; the grayscale of the otic capsule is 1694 (bright=bone) and the grayscale of membranous labyrinth (dark=labyrinth) is -114, thus setting the thresholding -114 and 1694 for this particular temporal bone.

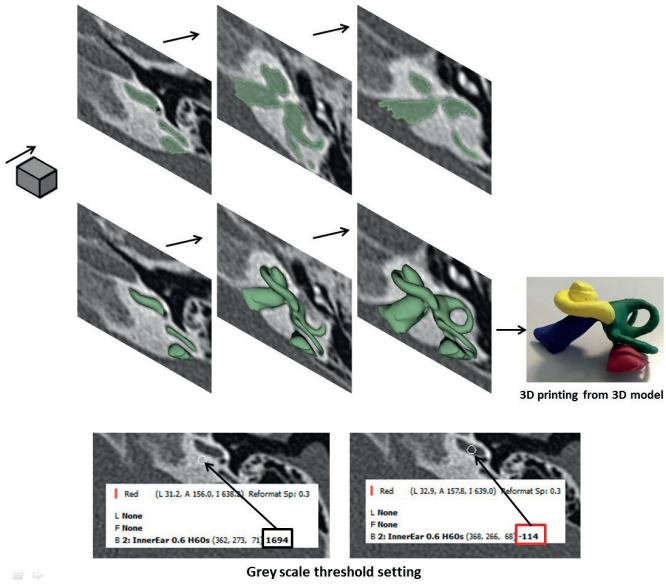

Figure 1. Segmentation is done by shading the areas of inner-ear structures from all image slices available, by setting a tight grayscale threshold. The 3D model from segmentation is transferred to the 3D printer to get the 3D printed model.

The cochlear portion alone was as well segmented from all data set in the interest of measuring its volume using the command "Segment statistics" from 3D slicer. A 3D model, which could be freely moved on the screen and viewed from all perspectives, was created. The VA could not be segmented from all temporal bones due to limited image resolution. Table 1 lists malformation types along with the number of cases identified under each malformation type and the volume of segmented cochlear portion alone. N/A corresponds to non-availability of more cases under that particular type.

3D printing of all inner-ear malformation types was made with a magnification factor of 2.8 using a Form-Labs (form 2) desktop 3D printer (Berlin, Germany) with photopolymer resin (white color) for educational purposes. Due to space limitations, not all images, but the selected, of the 3D-printed models are shown in this article.

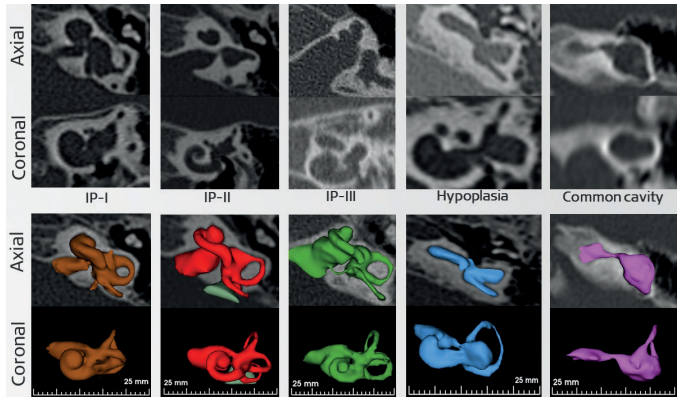

Figure 2. 2D and 3D images of all the inner-ear malformation types in both axial and coronal view, taking one sample from each malformation type.

Table 1. List of inner-ear malformation types identified along the number of cases under each type. Measured volume of the segmented cochlear portion alone is as well given

	Volume of the segmented cochlea (mm3)						
Cochlear Types	**Case 1**	**Case 2**	**Case 3**	**Case 4**	**Case 5**	**Avg.**	**Std. Dev.**
Normal anatomy	87.55 (R)	91.25 (R)	103.73 (L) (EVAS with norma anatomy cochlea)	n/a	n/a	95.64	11.44
IP type I	121.41 (L)	89.04 (L)	87.03 (R)	n/a	n/a	105.22	22.88
IP type II	51.50 (L)	96.49 (L)	35.24 (L)	29.37 (R)	n/a	73.99	31.81
IP type III	85.75 (L)	81.10 (R)	89.65 (L)	n/a	n/a	83.42	3.20
CC	178.91 (L)	165.4 (L)	232.34 (R)	233.4 (L)	52.48 (R)	172.15	9.56
CH	151.94 (L)	19.72 (L)	120.85 (R)	52.01 (R)	24.59 (R)	85.83	93.49

L: Left; R: Right; n/a: Non-availability of the sample. IP: Incomplete Partition; CC: Common Cavity; CH: Cochlear Hypoplasia

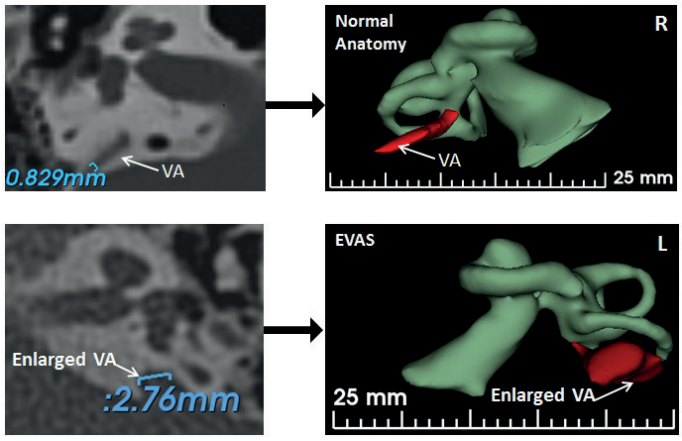

Figure 3. Width of VA is compared between the normal anatomy and EVAS.

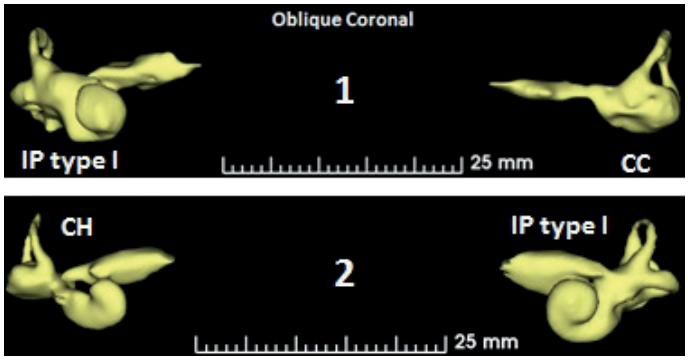

Figure 4. Dissimilar malformation types on each from two cases.

RESULTS

From HRCT/MRI data, we were able to identify inner-ear malformation types including Enlarged Vestibular Aqueduct Syndrome (EVAS), incomplete partition (IP) type-I, II (Mondini's deformity) and III (x-linked), common cavity (CC), and cochlear hypoplasia (CH). Segmentation of the complete inner-ear structures from the clinical image data sets took around 10 minutes as most of the data set had around 50 image slices covering the entire portion of inner-ear structures. Figure 1 shows the segmentation process followed by 3D printing.

A complete picture of all inner-ear malformation types both in two-dimensional (2D) CT images and 3D is given in Figure 2. Individual variation in size, shape, anatomy, and number of SCCs availability from each malformation type is given in Table 2.

3D Visualization and Analysis

EVAS: The EVAS that had near-normal cochlear anatomy (refer Table 2) had the width of VA around 2.76 mm. Volume of normal anatomy cochlea and the cochlea from EVAS was measured to be 87.55 mm^3 and 103.73 mm^3 respectively. As shown in Figure 3, the IAC of normal anatomy cochlea appears to be wider than IAC from EVAS at least from the data set available in this study.

IP type I: From the three data sets available under IP type I malformation, the volume of segmented cochlea appears to be very much comparable to normal anatomy cochlea. VA from sample 1 looks more like cylindrical; whereas with sample 3, it appears to be more triangular in shape. With sample 2, IAC appears much wider than other two samples.

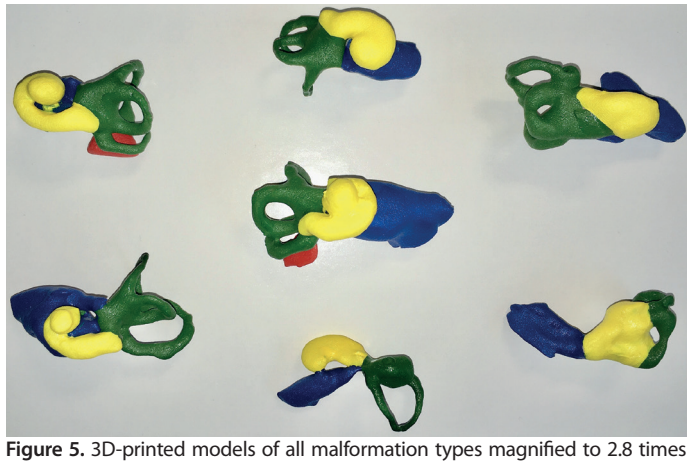

Figure 5. 3D-printed models of all malformation types magnified to 2.8 times the real size.

IP type II: From the four data sets available under this type, the volume of segmented cochlea is relatively lower than normal anatomy cochlear volume. Sample 2 had an enlarged VA. Samples 3 and 4 had a much wider IAC and slimmer cochlea, which is obvious from the lower volume of segmented cochlea. Sample 1 had only one SCC whereas all the other samples had three SCCs.

IP type III: From the three data sets available under this type, the volume of segmented cochlea measured to be more or less similar. The width of IAC from all three samples was much broader than the normal anatomy cochlea.

Common Cavity: From the five data sets available under this malformation type, the volume of common cavity (cochlea and vestibular organ collectively) varies significantly, with the lowest volume of 52.48 mm^3 for the smallest cavity (sample 5) to 233.40 mm^3 for the biggest cavity (sample 4). Sample 5 appeared to be the smallest with complete absence of all SCCs, whereas sample 3 had all three SCCs. Sample 1, 2, and 4 had one SCC. The connection between IAC and cavity is very thin as seen from sample 5, which could pose a serious question if this thin nerve is good enough to carry electrical signal if this cochlea gets a CI.

Cochlear Hypoplasia: Five data sets were available under this malformation type. None of the sample in this type looked similar. Samples 2 and 5 had the least volume of segmented cochlea as its size appeared very small in comparison to other samples. Samples 1 and 3 had pretty good sized cochlea. Interesting to note that sample 3 lacked all three SCCs, whereas sample 4 had one SCC and samples 1 and 2 had three SCCs. The size of IAC also varied a lot among the samples.

Dissimilar Malformations in Each Ear of Same Individuals

It was interesting to find dissimilar malformation types on each side from two cases. In case 1, it was IP type I on the right side and CC on the left side; and in case 2, it was cochlear hypoplasia on right side and IP type I on left side. Please refer Figure 4.

3D-printed models: For educational purposes, we did 3D printing of all malformation types with 2.8 times magnified from the segmented 3D model using a desktop 3D printer; and as shown in Figure 5, it came out pretty good. It is interesting to note that the size and shape

Table 2. 3D model of all inner-ear malformation types (refer to Table 1) given in both axial and coronal view. Volume of segmented cochlea was measured from the 3D slicer software using respective command

Nr.	Axial view	Coronal view	Segmentation of cochlear portion alone	Volume of segmented cochlea (mm^3)
Normal Anatomy (NA)				
1	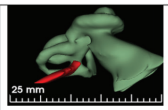	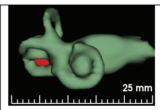	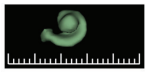	87.55
Enlarged Vestibular Aqueduct Syndrome (EVAS)				
1	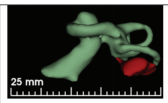	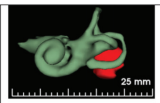	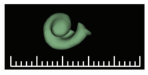	103.73
Incomplete Partition type I (IP-I)				
1	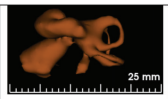	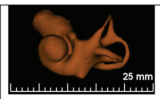	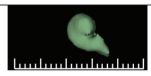	121.41
2	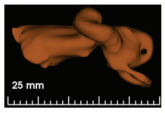	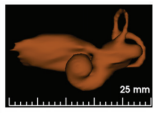	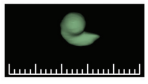	89.04
3	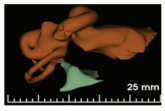	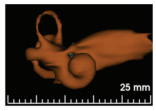	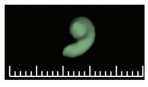	87.03
Incomplete Partition type II (Mondini's deformity) (IP-II)				
1	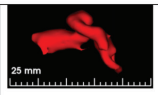	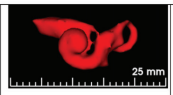	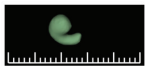	51.50
2	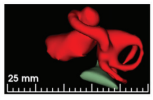	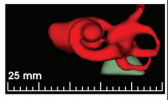	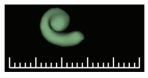	96.49
3	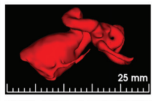	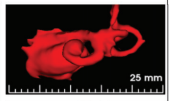		35.24
4	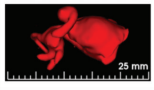	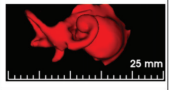		29.37
Incomplete Partition type III (X-linked)				
1	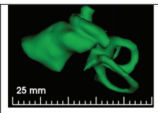	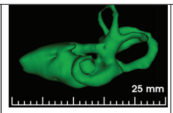	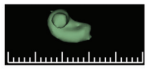	85.75
2	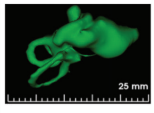	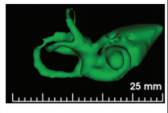		81.10
3	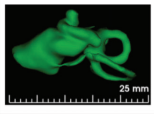	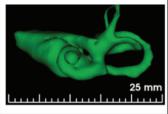	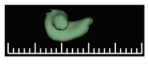	89.65
Common Cavity (CC)				
1	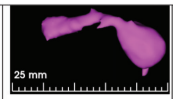	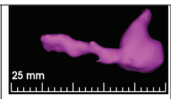	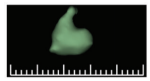	178.91
2	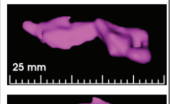	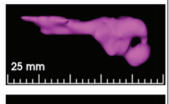	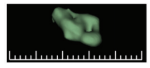	165.39
3	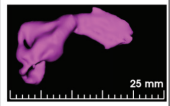	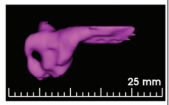	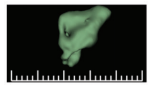	232.34
4	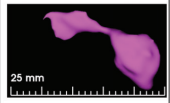	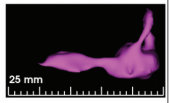	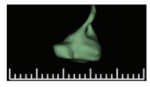	233.40
5	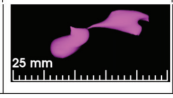	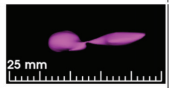	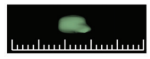	52.48
Cochlear Hypoplasia (CH)				
1	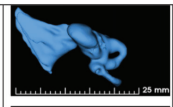	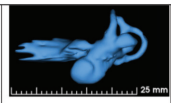	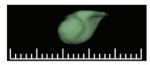	151.94
2	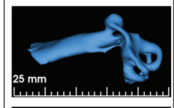	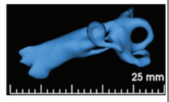	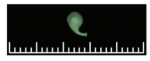	19.72
3	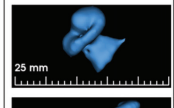	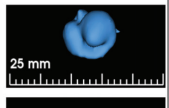	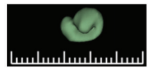	120.85
4	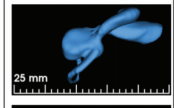	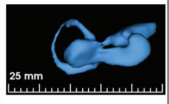	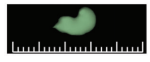	52.01
5	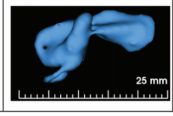	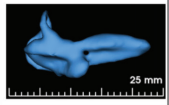	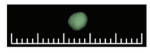	24.59

Table 3. List of previous studies captured cochlear malformation in 3D

S. No	Study reference	Types of cochlear malformation reported
1	Liu et al [15]	IP Type I, II, CC, and CH
2	Booth TN et al [18]	IP type II
3	Hara et al [19]	CH
4	Klingebiel R et al [20]	CH
5	Isono et al [21]	CH
6	Ma H et al [22]	CC, IP I, and II
7	Song JW et al [23]	IP, hypoplasia

IP: Incomplete Partition; CC: Common Cavity; CH: Cochlear Hypoplasia.

variation among different structures from malformation types was also seen from volumetric analysis given in Table 2.

DISCUSSION

We captured all the inner-ear malformation types so far reported in 3D from clinical CT/MR images of patient cases that were shared for educational purposes by various clinics across the world. Sennaroglu et al [3] did capture all the inner-ear malformation types in 2D from clinical images, but they mentioned nothing about 3D visualization. Liu et al [15] showed 3D model of CC, IP-I, IP-II, and CH, but malformation types including EVAS, CC, and IP type III were not mentioned. Yinn et al [16] covered nicely all the cochlear-vestibular malformation

types from pre-operative 2D radiographic images but again not in 3D as given in this study. Table 3 summarizes the list of previous studies that reported on 3D visualization in cochlear malformation. It is clear from this table that none of the previous studies ever covered all the malformation types in 3D as we did in this study.

As reported in literature with normal anatomy cochlea/patent cochlea [2], the variations in size and shape of inner-ear structures of all malformation types were significant depending on type and degree of malformation. This was well captured with the help of 3D segmentation. The VA was clearly visualized in five cases, and its width as given in axial plane and shape showed a great variation in comparison to the width of VA of normal anatomy cochlea [17]. The CH and CC types showed significant variations in the overall size and shape of all the structures in comparison to all other malformation types. This was nicely supported by the volumetric analysis of cochlear part alone that showed significant variation. The volume of CH varied too much in comparison to normal anatomy cochlea with the smallest and the biggest volumes being measured 19.72 mm^3 and 151.94 mm^3. Depending on the malformation types, the SCCs varied widely in its presence, size, and number. The thickness and the shape of IAC were varying too much, which can be visualized from the images with same scale in Table 2. Case 5 under common cavity malformation type given in Table 2 had thin connection between the cavity and IAC that would need more assessment to find if the thin nerve is potent enough to carry electrical stimulation to the brain.

Anything that could help an average experienced surgeon in better understanding patient's cochlear anatomy should be welcomed; and in that context, the 3D visualization of inner-ear malformation types could be beneficial to surgeons who are quite new to CI field especially in knowing overall size, shape, and the availability of inner-ear structures. Spending additional 10 min in segmenting the inner-ear structures as a part of pre-operative planning is worth the effort especially when treating pediatric cases with malformation. Considering numerous young/new CI surgeons coming into CI field, 3D segmentation of the labyrinth and IAC prior to surgery can improve accurate identification of malformation types and provide operating surgeon with better 3D understanding of the deformity. The 3D printing of anatomical structures have already shown to be beneficial in several medical applications [14]; and in that aspect, 3D-printed models of inner-ear malformation types will prove to be beneficial in the CI application especially while communicating with patients.

CONCLUSION

A good 3D understanding on the structures of inner-ear could be helpful especially for young CI surgeons who are new to the CI field. As demonstrated in this study, 3D visualization improves the clinicians' ability to visualize cochlear anatomy and the nearby structures compared to 2D images. Volumetric analysis showing a huge variation in the size of cochlear part from the complete inner-ear structures is yet another proof that no cochlea is similar in its size, shape, and the anatomy.

Ethics Committee Approval: No patients were involved at any point of time and therefore no ethics committee approval was necessary to perform this study.

Informed Consent: Informed consent was not needed for this study since all image datasets were anonymized even to the authors of this study.

Peer-review: Externally peer-reviewed.

Author Contributions: Concept – A.D.; Design - A.D., A.Dietz, C.J.; Supervision – P.R.; Resource – A.D., A.Dietz; Materials - A.D., A.Dietz; Data Collection and/or Processing – A.D., A.Dietz; Analysis and/or Interpretation – A.D., A.Dietz, PR; Literature Search – A.D., C.J.; Writing – A.D., A.Dietz, C.J., P.R.; Critical Reviews – A.Dietz, P.R.

Acknowledgements: The authors thank Ms. Francesca Maule, PhD (MED-EL) for her kind support with assistance in 3D segmentation using the 3D slicer. Mr. Roman Welzl and Ms. Anita Gruber from MED-EL are acknowledged for their support with 3D printing of the models. Prof. Levent Sennaroglu (Ankara, Turkey) is specially acknowledged for his teaching on cochlear malformation in general to the first author on various occasions that motivated to perform this study.

Conflict of Interest: AD and CJ are employed by MED-EL GmbH at the time of writing this manuscript. No other conflict of interest declared by the authors.

Financial Disclosure: The authors declared that this study had received no financial support.

REFERENCES

1. Sarant JZ, Harris DC, Galvin KL, Bennet LA, Canagasabey M, Busby PA. Social development in children with early cochlear implants: Normative comparisons and predictive factors, including bilateral implantation. Ear Hear 2018; 39: 770-82. **[CrossRef]**
2. Erixon E, Högstorp H, Wadin K, Rask-Andersen H. Variational anatomy of the human cochlea: implications for cochlear implantation. Otol Neurotol 2009; 30: 14-22. **[CrossRef]**
3. Sennaroğlu L, Bajin MD. Classification and Current Management of Inner Ear Malformations. Balkan Med J 2017; 34: 397-411. **[CrossRef]**
4. Sun B, Dai P, Zhou C. Study on 2747 cases of inner ear malformation for its classification in patient with sensorineural hearing loss. Lin Chung Er Bi Yan Hou Tou Jing Wai Ke Za Zhi 2015; 29: 45-7.
5. Sennaroglu L, Saatci I. A new classification for cochleovestibular malformations. Laryngoscope 2002; 112: 2230-41. **[CrossRef]**
6. Fishman AJ, roland JT Jr, Alexiades G, Mierzwinski J, Cohen NL. Fluoroscopically assisted cochlear implantation. Otol Neurotol 2003; 24: 882-6. **[CrossRef]**
7. Graham J, Phelps P, Michaels L, Path F. Congenital malformations of the ear and cochlear implantation in children: review and temporal bone report of common cavity. J Laryngol Otol Suppl 2000; 25: 1-14. **[CrossRef]**
8. Aschendorff A, Marangos N, Laszig R. Large vestibular aqueduct syndrome and its implications for cochlear implant surgery. Am J Otol 1997; 18: S57.
9. Nauman FM, Wick CC, Wahba M, Gupta A, Piper R, Murray GS, et al. Bilateral sequential cochlear ımplantation in patients with enlarged vestibular aqueduct (EVA) syndrome. Otol Neurotol 2016; 27: e96-103. **[CrossRef]**
10. Kontorinis G, Goetz F, Giourgas A, Lenarz T, Lanfermann H, Giesemann, AM. Radiological diagnosis of incomplete partition type I versus type II: significance for cochlear implantation. Eur Radiol 2012; 22: 525-32. **[CrossRef]**
11. Incesulu A, Vural M, Erkam U, Kocaturk S. Cochlear implantation in children with inner ear malformations: report of two cases. Int J Pediatr Otorhinolaryngol 2002; 65: 171-9. **[CrossRef]**
12. Beltrame MA, Birman CS, Cervera EJ, Kassouma J, Manolidis S, Pringle MB, et al. Common cavity and custom-made electrodes: Speech perception and audiological performance of children with common cavity implanted with a custom-made MED-EL electrode. Int J Pediatr Otorhinolaryngol 2013; 77: 1237-43. **[CrossRef]**
13. Chan HHL, Siewerdsen JH, Vescan A, Daly MJ, Prisman E, Irish JC. 3D rapid prototyping for otolaryngology-head and neck surgery: Applications in image-guidance, surgical simulation and patient specific modeling. Plos One 2015; 10: e0136370. **[CrossRef]**

14. Tack P, Victor J, Gemmel P, Annemans L. 3D-printing techniques in a medical setting: a systematic literature review. 2016; 15: 115. [CrossRef]
15. Liu YK, Qi CL, Tang J, Jiang ML, Du L, Li ZH, et al. The diagnostic value of measurement of cochlear length and height in temporal bone CT multiplanar reconstruction of inner ear malformation. Acta Otolaryngol 2017; 137: 119-26. [CrossRef]
16. Yiin RS, Tang PH, Tan TY. Review of congenital inner ear abnormalities on CT temporal bone. Br J Radiol 2011; 84: 859-63. [CrossRef]
17. Lee KH, Lee J, Isaacson B, Kutz W, Roland PS. Cochlear implantation in children with enlarged vestibular aqueduct. Laryngoscope 2010; 120: 1675-81. [CrossRef]
18. Booth TN, Wick C, Clarke R, Kutz JW, Medina M, Gorsage D, et al. Evaluation of the normal cochlear second interscalar ridge angel and depth on 3D T2-weighted images: A tool for the diagnosis of scala communis and incomplete partition type II. AJNR Am J Neuroradiol 2018; 39: 923-7. [CrossRef]
19. Hara M, Takahashi H, Kanda Y. The usefulness of reconstructed 3D images in surgical planning for cochlear implantation in a malformed ear with an abnormal course of the facial nerve. Clin Exp Otorhinolaryngol 2012; 5 Suppl 1: S48-52. [CrossRef]
20. Klingebiel R, Bockmühl U, Werbs M, Freigang B, Vorwerk W, Thieme N, et al. Visualization of inner ear dysplasias in patients with sensorineural hearing loss. Acta Radiol 2001; 42: 574-81. [CrossRef]
21. Isono M, Murata K, Nakayama K, Miyashita H, Tanaka H, Ishikawa M. Inner ear anamoly of three-dimensional computed tomography: computed tomographic attenuation and image changes. Acta Otolaryngol Suppl 2000; 542: 62-6. [CrossRef]
22. Ma H, Han P, Liang B, Tian ZL, Lei ZQ, Kong WJ, et al. Multislice spiral computed tomography imaging in congenital inner ear malformations. J Comput Assist Tomogr 2008; 32: 146-50. [CrossRef]
23. Song JW, Lee IS, Kim HJ, Goh EK, Kim LS. Congenital inner ear malformation: three dimensional volume rendering image using MR CISS sequence. J Korean Radiol Soc 2003; 49: 237-43. [CrossRef]